Catalysis Science & Technology

ROYAL SOCIETY OF CHEMISTRY

PAPER

View Article Online
View Journal | View Issue

Cite this: *Catal. Sci. Technol.*, 2025, **15**, 1644

Revealing the reaction mechanism of ammonia synthesis over bimetallic nitride catalyst from a kinetic perspective†

Shuairen Qian,[a] Zhengwen Li,[a] Xiaohang Sun,[a] Yuxin Chen,[a] Kai Feng,[ab] Kaiqi Nie,[a] Binhang Yan *[a] and Yi Cheng *[a]

Ammonia is one of the most important feedstocks for both fertilizer production and energy carriers. Identifying the appropriate reaction mechanism from the multiple pathways of ammonia synthesis is critical to the rational design of efficient catalysts. However, the low adhesion of nitrogen molecules hinders the observation of the behavior of reaction intermediates and the understanding of the reaction mechanisms. Kinetic analysis is a powerful tool to recognize reaction mechanisms, but it is difficult to expand case-by-case research to target systems. Herein, we establish a framework for the investigation of reaction mechanisms based on kinetic analysis and apply it to ammonia synthesis over a Co_3Mo_3N bimetallic nitride catalyst. The energetics of elementary reactions calculated by density functional theory (DFT) is used for a microkinetic model to obtain information about reaction mechanisms. Theoretical calculations indicate that the reaction rate *via* the surface reaction mechanism is much higher than that *via* the MvK mechanism. Nitrogen-vacancy-generation-induced charge redispersion is the major hindrance to the subsequent hydrogenation of NH_x species for the MvK mechanism. This information guides the design and analysis of kinetic experiments. A series of steady-state and transient kinetic experiments demonstrate the dominant role of the dissociation mechanism over associative and MvK mechanisms. The low coverage of surface N species derived from both DFT-based microkinetic simulations and transient kinetic experiments originates from the high energy barrier to N_2 dissociation. This work reveals the reaction mechanism of ammonia synthesis over bimetallic nitrides based on both theoretical calculations and experimental results and proposes a new paradigm for elucidating reaction mechanisms in heterogeneous catalysis from a kinetic perspective.

Received 9th November 2024,
Accepted 24th January 2025

DOI: 10.1039/d4cy01359j

rsc.li/catalysis

1. Introduction

Ammonia (NH_3) is an extremely valuable nitrogen-containing molecule in the nitrogen cycle and transformations.[1–3] NH_3 as a nitrogen fertilizer has been used to feed thousands of the world's population in the past century.[4] In recent years, NH_3 has played an increasingly important role as an energy carrier.[5–7] Industrial NH_3 is produced mainly through the Haber–Bosch process, which is operated at high temperature (400–600 °C) and high pressure (20–40 MPa).[8,9] Fe- and Ru-based catalysts, as traditional ammonia catalysts, are generally believed to follow the dissociation mechanism. Therefore, the harsh conditions of ammonia synthesis stem from thermodynamic and kinetic characteristics, in particular the difficulty of breaking the N≡N triple bond.[10–12] Many studies have been devoted to weakening the N≡N bond through electron transfer from the catalyst surface to the antibonding orbitals of N_2 molecules, such as the addition of alkali metal promoters,[13] the construction of electron-rich centers,[14–17] and assistance from external fields.[18,19] Defect engineering mediated by nitrogen (N) vacancies is another effective approach to accelerate the reaction process.[20–23] Similar to oxygen vacancies, the electrons located at the nitrogen vacancies are favorable for N_2 activation.[20–22,24] Transition metal nitrides are considered a class of potential catalysts with abundant lattice defects and they can generate ammonia through the activation and regeneration of lattice N, *i.e.*, the Mars–van Krevelen (MvK) mechanism.[25–27] In addition, an ensemble of metal sites with their electronic structure modulated by N heteroatoms is also accessible on the catalyst surface of metal nitrides. These metal sites, depending on nitrogen affinity, can also play a vital role in N_2 dissociation (Fig. 1).[28,29] However, due to the weak adhesion

[a] *Department of Chemical Engineering, Tsinghua University, Beijing 100084, P. R. China. E-mail: binhangyan@tsinghua.edu.cn, yicheng@tsinghua.edu.cn*
[b] *Institute of Functional Nano & Soft Materials (FUNSOM), Soochow University, Suzhou, Jiangsu 215123, P. R. China*

† Electronic supplementary information (ESI) available. See DOI: https://doi.org/10.1039/d4cy01359j

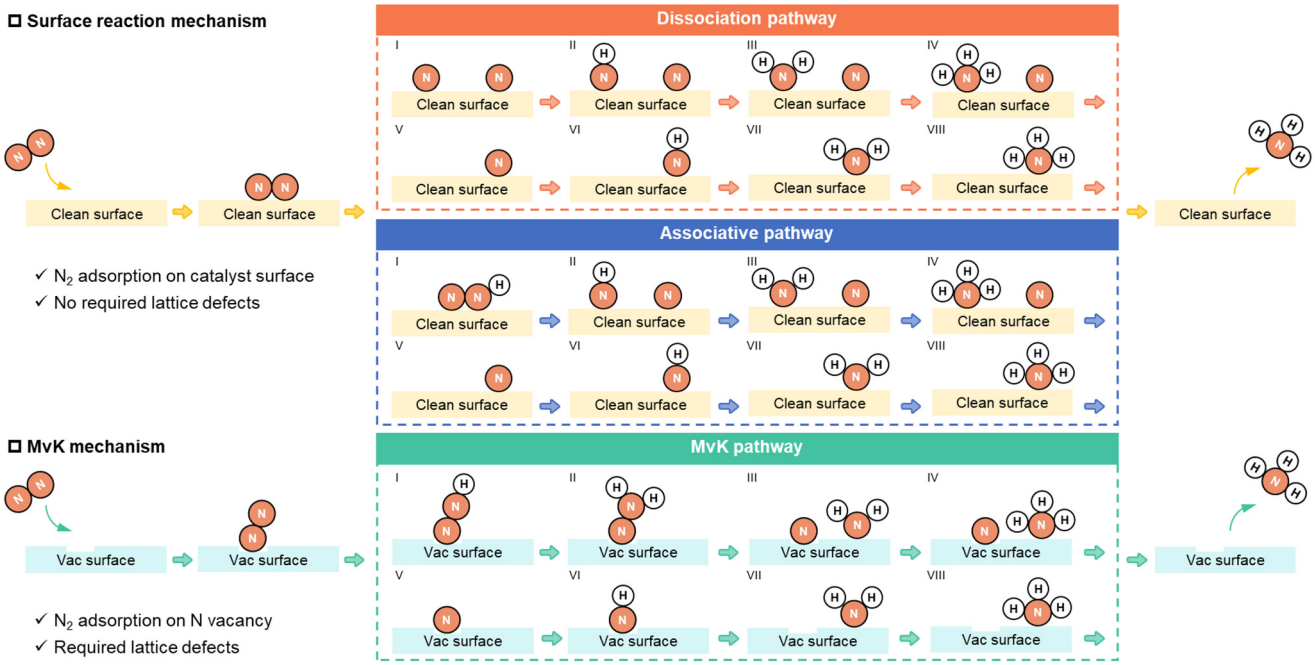

Fig. 1 Schematic depiction of the reaction mechanism for ammonia synthesis.

of N_2 molecules to catalyst surfaces, it is difficult to determine the behavior and transformations of the intermediate species using well-developed spectroscopic tools. As a result, the reaction mechanisms and coexistence of two pathways contributing to ammonia production on nitride surfaces have not yet been precisely and intuitively identified by spectroscopic methods. Kinetic analysis is a powerful tool to identify the behavior of reaction intermediates and to understand reaction mechanisms.[30,31] In particular, transient kinetic analysis, in contrast to steady-state kinetic analysis, where rate expressions derived based on microkinetic are fitted with experimental data, allows for the mathematical manipulation of transient response signals to obtain abundant information about reaction mechanisms.[32–34] Many kinetic investigations on ammonia synthesis and other processes have been reported.[16,35–43] Nevertheless, these studies have been conducted on a case-by-case basis without establishing a systematized procedure. It is essential to establish a complete framework based on kinetic analysis and to apply it to target catalytic reaction systems.

Herein, we establish a framework for the investigation of reaction mechanisms based on kinetic analysis and apply it to ammonia synthesis over metal nitride catalysts. The electron energy calculated from density functional theory (DFT) is used as the initial value for solving a mean-field microkinetic model (MKM), and information on reaction mechanisms (*e.g.*, the rate-determining step) and the coverage of surface species is used to guide the design and analysis of kinetic experiments. Combining steady-state and transient kinetics, we identify the reaction mechanisms and the contributions of different pathways, and apply the mechanisms to catalyst design and larger scale applications. In this work, a Co_3Mo_3N bimetallic nitride catalyst, with both metal sites favoring N_2 dissociation and electron-enrichment of lattice N sites, is chosen as a model nitride catalyst.[28,44–46] Ammonia production over the Co_3Mo_3N catalyst *via* different reaction pathways is identified by both microkinetic models and transient kinetics analysis. The rate-determining step (RDS) obtained from degree of rate control (DRC) analysis is applied to the derivation of rate expressions. A series of isotope experiments demonstrate that ammonia synthesis *via* the dissociation mechanism shows higher reactivity than that *via* the MvK mechanism. Defective charges promote N_2 activation but inhibit hydrogenation of NH_x species. Steady-state isotopic-transient kinetic analysis (SSITKA) experiments reveal the low surface coverage and turnover frequency of dissociation mechanism intermediates on the catalyst surface. Overall, this framework combining theoretical calculations and experimental measurements from a kinetic perspective serves as a powerful tool for the elucidation of reaction mechanisms.

2. Results and discussion

2.1 Reaction mechanism identification

A large amount of research has concluded that the reaction mechanism of ammonia synthesis on nitride surfaces follows the MvK mechanism, and that the defect-regeneration behavior of lattice N is crucial for N_2 activation and subsequent hydrogenation.[20–22] Nevertheless, the CoMo2 ensemble on the Co_3Mo_3N surface creates opportunities for the occurrence of a classical dissociation pathway or even associative pathways (Fig. 1).[44–46] All the surface CoMo2 sites were traversed by intermediate species adsorptions and

transition state searches and all of these surface sites are equivalent (see the section Calculation tests in ESI† for details). In addition, the configurations of all intermediate species were also determined by structural optimization (Fig. S5 and Table S1†). Based on the reaction mechanisms for ammonia synthesis, the potential energy profiles on the Co_3Mo_3N catalyst were calculated, as shown in Fig. 2a. Due to the presence of several different intermediate species for N–N bond dissociation, associative pathways are extremely complex and contain large reaction networks (Fig. S6†). All associative pathways were investigated, as shown in Fig. S10–S18.† After the first N_2 hydrogenation process, the dissociation process of NNH* into NH* and N* is energetically more favorable (0.25 eV) compared to further hydrogenation to generate HNNH* (1.00 eV) and NNH_2^* (1.09 eV). This result confirms that it is difficult for continuous hydrogenation similar to enzymatic processes in heterogeneous catalysis for ammonia synthesis.[9,47,48] Therefore, an associative pathway *via* NNH* intermediate species is considered to be a candidate for an associative mechanism. Direct N_2 dissociation also occurs easily on the CoMo2 sites due to the Sabatier optimal of Co–Mo predicted by the volcano curve.[35,49] Both the dissociation pathway and the associative pathway are surface reaction mechanisms and the hydrogenation process for surface NH_x^* species is identical, and completely different from the lattice

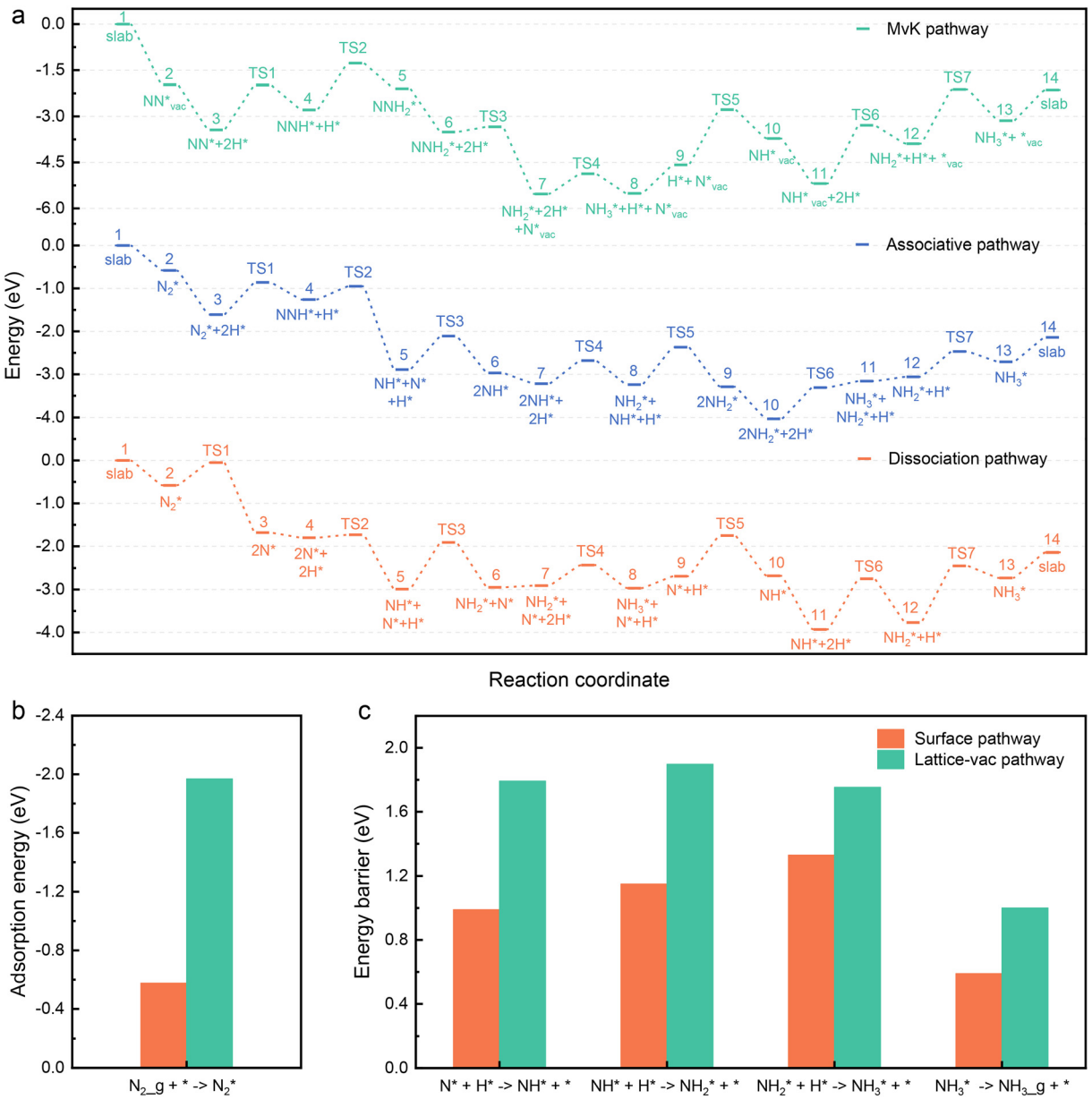

Fig. 2 Reaction mechanisms and DFT energetics. (a) Calculated potential energy profile of NH_3 synthesis for the Co_3Mo_3N catalyst *via* the dissociation pathway, associative pathway and MvK pathway. * represents the surface site and $*_{vac}$ represents the N vacancy site. DFT energetics for (b) N_2 adsorption and (c) hydrogenation process of N adsorption species.

N-mediated MvK mechanism. For the MvK mechanism, N_2 adsorption occurs on the N vacancy, and the surface N species hydrogenation process occurs on a defective surface rather than on a clean surface. Lattice vacancies are more capable of N_2 adsorption due to the formation of covalent interactions between surface Mo atoms and N (Fig. 2b). Nevertheless, barriers to the hydrogenation of NH_x^* species and NH_3^* desorption on the defective surface are much higher than those on a clean surface, leading to the potentially unfavorable occurrence of ammonia synthesis *via* a lattice-vac pathway (Fig. 2c).

To further validate the potential reaction mechanism on the Co_3Mo_3N catalyst, we performed mean-field microkinetic modelling based on the above DFT-calculated potential energy surfaces, as illustrated in Fig. 3. The reaction rate heatmaps of other associative pathways were investigated, as shown in Fig. S10–S18.† The NNH* associative pathway exhibits more significant reactivity than the other associative pathway, which is consistent with the above analysis based on the energy barriers of the key elementary steps. Mixed pathways with different associative intermediates were also considered, to observe the potential reaction fluxes (Fig. S22†). Interestingly, all contributions to ammonia production in mixed pathways originate from the NNH* associative pathway. Therefore, the NNH* associative pathway is more favorable and the associative mechanism is denoted as the NNH* associative pathway in subsequent studies. The reaction rates (in terms of TOF) *via* the dissociation mechanism and associative mechanism show significant temperature sensitivity, as illustrated in Fig. 3d. In low-temperature regions, the associative pathway has higher reactivity for ammonia synthesis. In high-temperature regions, the dissociation pathway dominates the reaction contribution. In contrast, the MvK pathway exhibits four orders of magnitude lower intrinsic activity under conventional reaction conditions. Degree of rate control (DRC) analysis was performed to determine the rate-determining step (RDS) for different reaction pathways (Fig. S23†). N_2^* dissociation and N_2^* hydrogenation processes are the RDS for the dissociation pathway and associative pathway, respectively. The RDS of the MvK pathway is the NH_2^* hydrogenation process. Thus, the low activity can be attributed to the hydrogenation-blocking behavior exhibited in Fig. 2c, which seems to contradict previous reports on

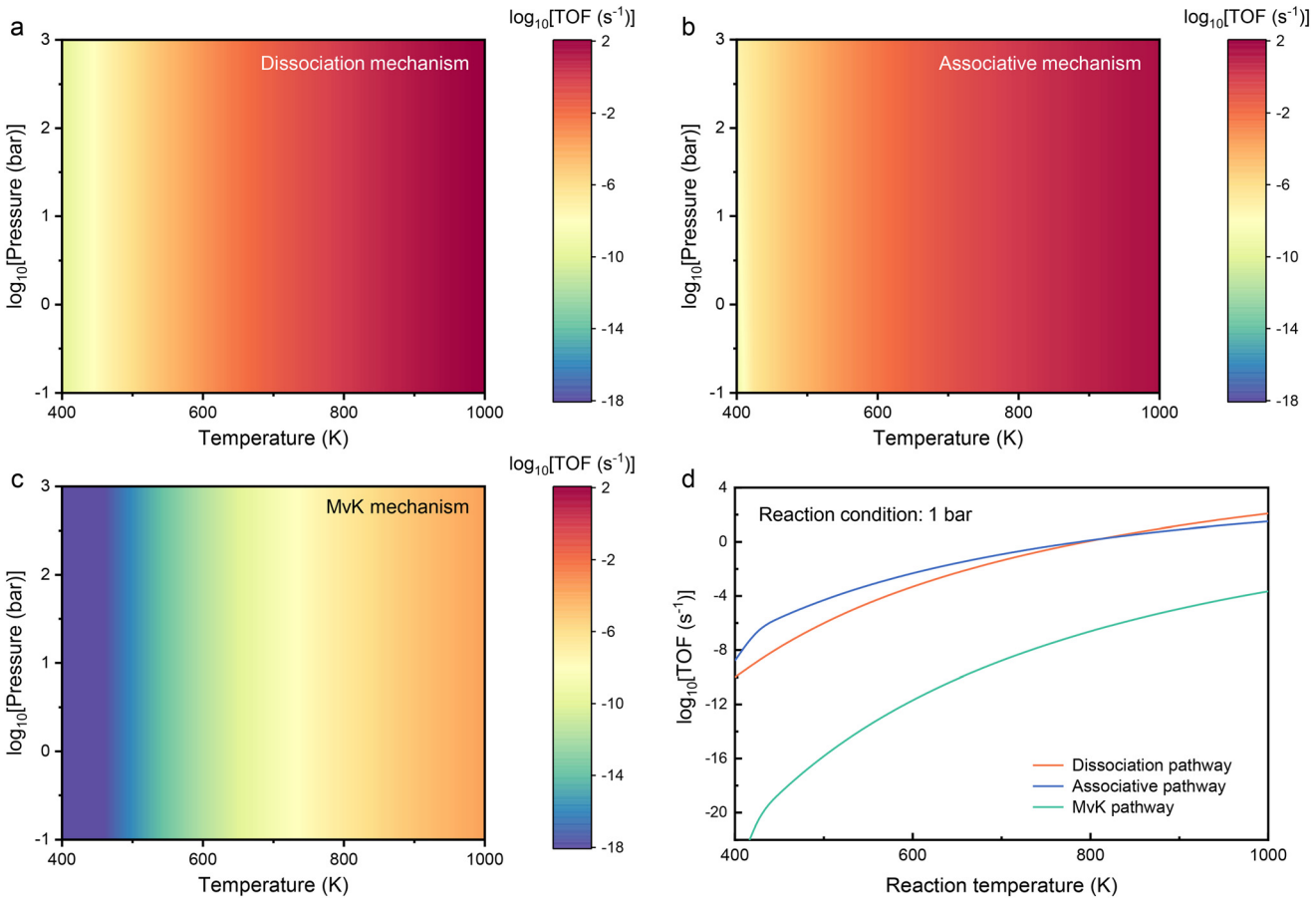

Fig. 3 Reaction performance based on the microkinetic model. Ammonia synthesis rate (TOF) as a function of temperature and pressure at N_2/H_2 = 1/3 for the Co_3Mo_3N catalyst *via* (a) the dissociation pathway, (b) the associative pathway and (c) the MvK pathway. (d) Ammonia synthesis rate for different reaction mechanisms as a function of temperature at 1 bar and N_2/H_2 = 1/3.

lattice-N-mediated ammonia synthesis performance over a Co_3Mo_3N catalyst.[28,50]

2.2 Electronic structure perspectives on the reaction mechanism

We performed an electronic structure analysis of the clean surface and defective surface to gain insight into the origin of the low reactivity for the MvK mechanism (Fig. 4). Density of states (DOS) calculations were carried out on the clean surface and the defective surface (Fig. 4a). The creation of N vacancies causes a redistribution of electrons around the Fermi energy level, upshifting the d band center of Mo coordinated to lattice N. The higher energy of the Mo 4d band center induces stronger interactions with surface NH_x^* species, rendering the hydrogenation inert. This behavior is similarly confirmed by charge analysis. The accumulated charge located in the N vacancy on the defective surface is redistributed, causing a more electron-rich Mo center and generating stronger binding capacity to the surface species (Fig. 4b–d). The charge density difference of N_2^* adsorption demonstrates a redistribution of electron density, and the adsorption strength depends on electron transfer (Fig. 4 and S25†). Similar to catalyst poisoning, stronger NH_x^* adsorption blocks the active sites on the catalyst surface. This phenomenon also puts the classical linear scaling relationship into perspective.[51,52]

2.3 Decoupling reaction mechanisms through steady-state and transient kinetics

Co_3Mo_3N bimetallic nitride is a special catalytic material with two types of active sites, the CoMo2 site and lattice N site, on the surface, which can realize ammonia production simultaneously through the surface reaction mechanism and the MvK mechanism (Fig. 5a).[46] We successfully synthesized Co_3Mo_3N pure-phase catalysts, as in previous reports (Fig. S26 and S27†).[29] To identify the contribution of different reaction mechanisms, TPSR experiments under different reaction atmospheres were carried out for the Co_3Mo_3N catalyst. As shown in Fig. 5b, the Co_3Mo_3N catalyst exhibits the same onset temperature (~230 °C) for both the N_2/H_2 reaction and the Ar/H_2 reaction, which can be attributed to the reaction of surface H species with lattice N. The NH_3 production contribution from residual surface NH_x species is considered within the MvK mechanism. Another low-temperature signal (~390 °C) was observed, suggesting the existence of two different types of lattice N coordination environment on the surface of the Co_3Mo_3N catalyst, in agreement with previous reports.[46,50] Identical induction-phase behavior suggests that the low-temperature activity originates from the MvK mechanism rather than the surface mechanism. As the temperature is further increased to the conventional reaction temperature interval, the surface reaction contribution plays a dominant role. Accordingly, the lattice exchange rate between lattice N and surface N is much lower than the surface exchange rate in $^{14}N_2$–$^{15}N_2$ isotope exchange experiments (Fig. 5c). The low exchange rate of lattice N corresponds to the low ammonia production flux *via* the MvK mechanism. Moreover, taking the coverage of lattice N as a benchmark, the coverage of surface N is five times lower than that of lattice N, but the reactivity *via* these intermediate species is reversed (Fig. 5d and S29†). This result will be discussed in detail later.

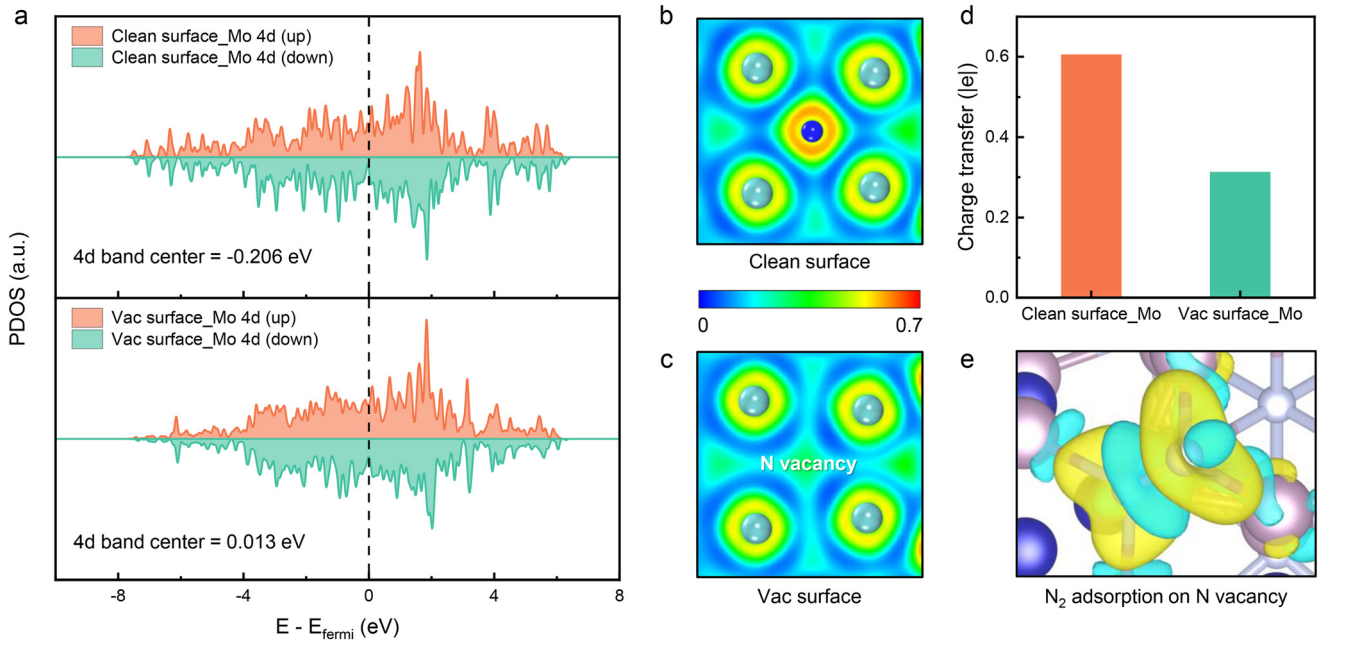

Fig. 4 Electronic structure analysis for reaction mechanisms. (a) Surface Mo 4d PDOS of the clean surface and the defective surface. Surface charge distribution of (b) the clean surface and (c) the defective surface. (d) Bader charge for surface Mo atom of the clean surface and the defective surface. (e) Top view of the charge density difference for N_2 adsorption on an N vacancy.

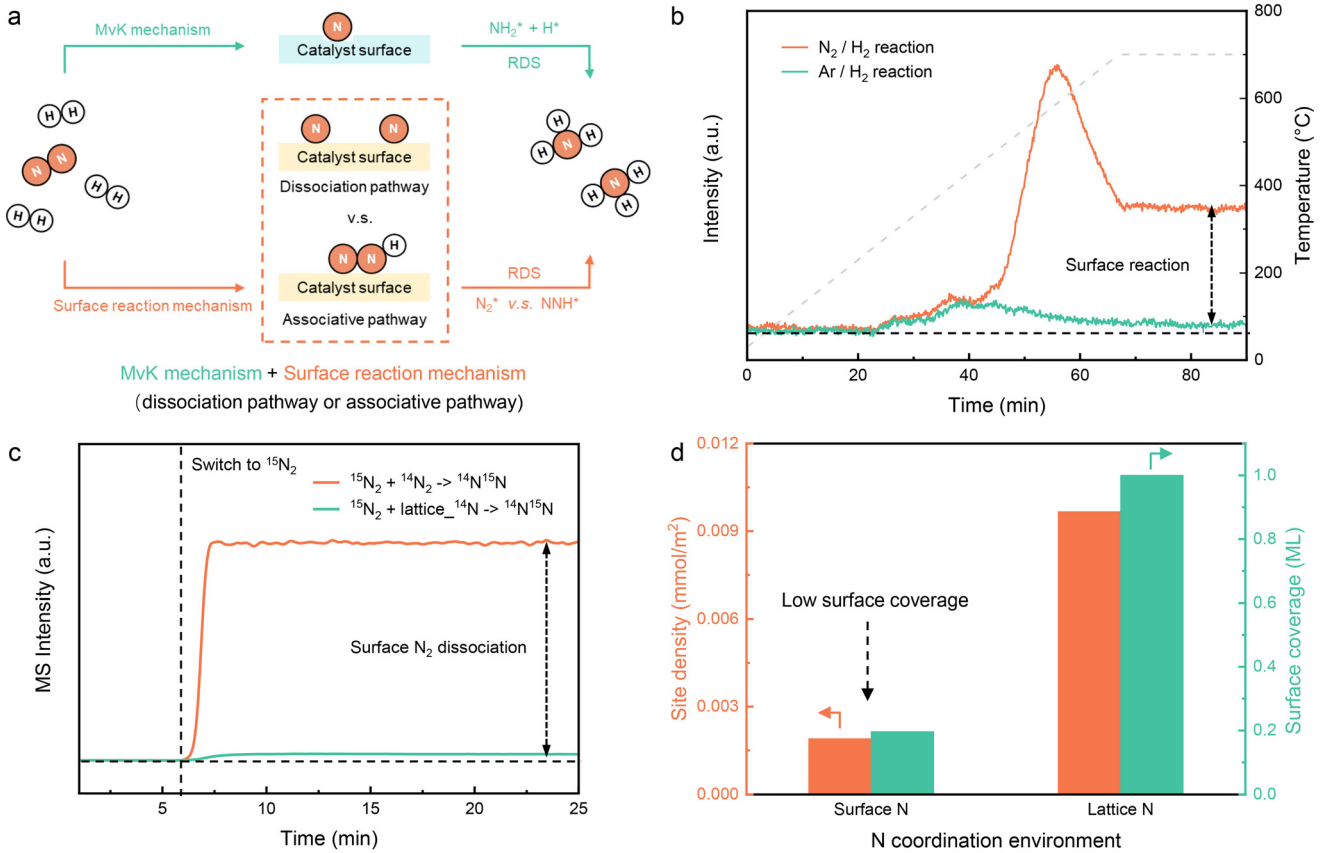

Fig. 5 Decoupling surface reaction mechanism and MvK mechanism. (a) A scheme showing reaction characteristics and surface species behavior for the surface reaction mechanism and the MvK mechanism. (b) Temperature-programmed surface reaction with different reaction feeds. (c) $^{14}N_2$–$^{15}N_2$ isothermal isotope exchange over the Co_3Mo_3N catalyst at 500 °C ($^{14}N_2$: $^{15}N_2$ = 4 : 1). (d) Surface site density and coverage for different N coordination environments based on SSITKA studies under 500 °C.

Furthermore, we investigated the critical pathways followed by surface mechanisms (Fig. 6a). According to microkinetic simulations, the RDS of the dissociation pathway and the associative pathway are N_2^* dissociation and N_2^* hydrogenation processes, respectively, and the essential difference lies in whether the surface H is directly involved in RDS or not, which would result in different kinetic behaviors. The H_2–D_2 isotopic reaction of ammonia synthesis was performed over the Co_3Mo_3N catalyst. An inverse isotope effect (k_H/k_D = 0.50) was observed experimentally, indicating that the hydrogenation step is not the rate-determining step (Fig. 6b). Similar experimental phenomena were previously found for ammonia synthesis *via* the dissociation mechanism over Fe-promoted catalysts.[53] Steady-state kinetic experiments were also performed to further confirm the reaction pathways (details are given in S6 Steady-state kinetic analysis in ESI†). The kinetic models were derived using the assumptions about the rate-determining step. The modelled reaction rate of the dissociation pathway gives a better fit to the experimental reaction rate than that of the associative pathway (Fig. 6c and d). We also derived kinetic models for the associative mechanism with a potential rate-determining step of NNH* dissociation and obtained a worse fit (Fig. S28†).[39] On the other hand, the N_2^* dissociation process can occur without the assistance of H_2 feed (Fig. 5c), suggesting that the dissociation pathway may be the potential reaction mechanism and that N_2^* is the most abundant surface intermediate due to the slow consumption of N_2^* imposed by N_2^* dissociation as the RDS.

Additional insights into the transient kinetics and behavior of surface N species over the Co_3Mo_3N catalyst were probed by steady-state isotopic-transient kinetic analysis (SSITKA) with an isotopic switch of $^{14}N_2$ to $^{15}N_2$ (Fig. 6e and S29†). $^{14}NH_3$ and $^{15}NH_3$ production signals were studied to obtain kinetic information. There is a slight delay in the decay of the $^{14}NH_3$ signal due to the transient release of NH_3 produced through lattice N during switching of the reaction gas. The continuous increase in the $^{15}NH_3$ signal shows that ammonia production is derived mainly from surface N rather than lattice N. In addition, isotope switching experiments at different temperatures were implemented to evaluate the kinetic behavior of the most abundant surface intermediate (Fig. S29†). Response curves at different temperatures show similar features, but a notable difference is the much longer residence time at high temperature. The behavior of the most abundant surface intermediate was determined by establishing the Arrhenius relationship. The intrinsic activation energy for

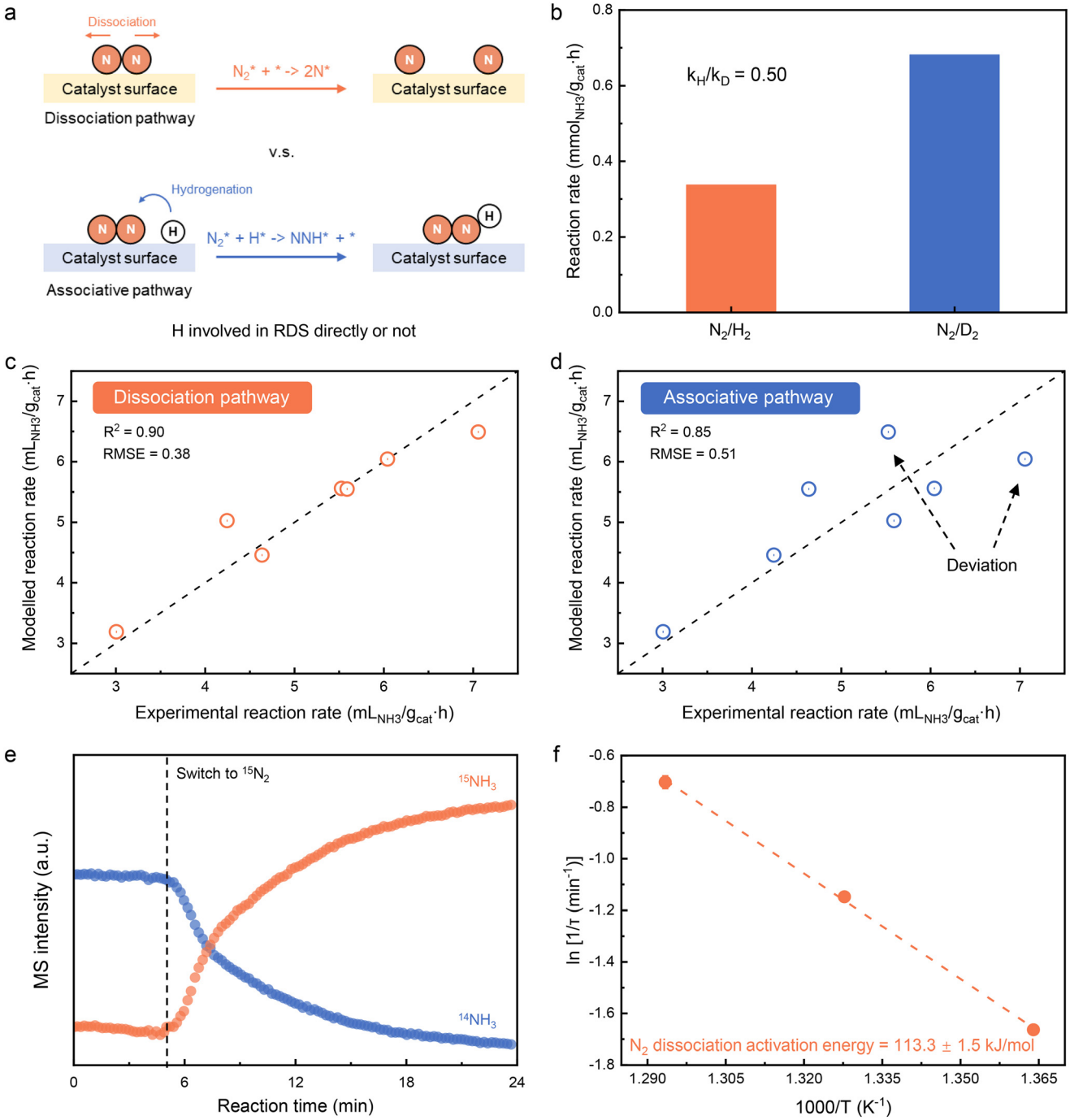

Fig. 6 Decoupling dissociation mechanism and alternating mechanism. (a) A scheme of reaction characteristics and behavior of surface species for the dissociation mechanism and the alternating mechanism. (b) H_2–D_2 isotopic reaction over the Co_3Mo_3N catalyst at 450 °C and 1 bar. Kinetic fit results of reaction rates for (c) the dissociation pathway and (d) the associative pathway. (e) $^{14}NH_3$–$^{15}NH_3$ product signals during the switching process of SSITKA studies. (f) Arrhenius-type plot for key intermediate species based on SSITKA studies.

the N_2^* dissociation elementary step is 113.7 kJ mol^{-1}, which is higher than the apparent activation energy for steady-state ammonia synthesis (75.1 kJ mol^{-1}) over the Co_3Mo_3N catalyst (Fig. 6f and S31†). The hydrogenation process of N* species can be achieved rapidly compared to the N_2 dissociation process, which leads to the low abundance of surface N* species (Fig. 5d). Steady-state and transient kinetic analysis combined with theoretical calculations accurately identify the reaction mechanism of ammonia synthesis, which is expected to provide insights into a mechanistic understanding of such materials and practical applications at larger scales.

3. Conclusions

In summary, we have developed a framework for the investigation of reaction mechanisms based on kinetic analysis. Using this approach, we achieved the identification of the reaction mechanism for ammonia synthesis over a Co_3Mo_3N bimetallic nitride catalyst with dual sites. Ammonia synthesis *via* the surface reaction mechanism exhibits higher reactivity than that *via* the MvK mechanism, according to DFT calculations and microkinetic models. The redistribution of defective charges hinders the hydrogenation behavior of surface NH_x^* species. Microkinetic simulations provide insights into the design of kinetic experiments. Both steady-state and transient kinetic analysis show that ammonia synthesis is dominated by the surface reaction mechanism of the dissociation pathway. The high activation energy barrier for N_2 dissociation results in low coverage of surface N species. The combination of theoretical calculations and experimental results provides more detailed evidence to elucidate the reaction mechanism in heterogeneous catalysis. This study provides a paradigm for the study of reaction mechanisms from a kinetic perspective.

Data availability

The data that support the findings of this study are available within the article and its ESI,† or from the corresponding author on reasonable request.

Conflicts of interest

The authors declare no competing financial interest.

Acknowledgements

This work is financially supported by the National Natural Science Foundation of China (No. 22278235, No. 21991104 and No. 22250710677) and International Joint Mission on Climate Change and Carbon Neutrality. This work is also supported by Tsinghua National Laboratory for Information Science and Technology.

References

1 J. G. Chen, R. M. Crooks, L. C. Seefeldt, K. L. Bren, R. M. Bullock, M. Y. Darensbourg, P. L. Holland, B. Hoffman, M. J. Janik, A. K. Jones, M. G. Kanatzidis, P. King, K. M. Lancaster, S. V. Lymar, P. Pfromm, W. F. Schneider and R. R. Schrock, *Science*, 2018, **360**, eaar6611.
2 D. R. MacFarlane, P. V. Cherepanov, J. Choi, B. H. R. Suryanto, R. Y. Hodgetts, J. M. Bakker, F. M. Ferrero Vallana and A. N. Simonov, *Joule*, 2020, **4**, 1186–1205.
3 D. Ye and S. C. E. Tsang, *Nat. Synth.*, 2023, **2**, 612–623.
4 J. W. Erisman, M. A. Sutton, J. Galloway, Z. Klimont and W. Winiwarter, *Nat. Geosci.*, 2008, **1**, 636–639.
5 J. Guo and P. Chen, *Chem*, 2017, **3**, 709–712.
6 N. Morlanés, S. P. Katikaneni, S. N. Paglieri, A. Harale, B. Solami, S. M. Sarathy and J. Gascon, *Chem. Eng. J.*, 2021, **408**, 127310.
7 S. Wu, N. Salmon, M. M.-J. Li, R. Bañares-Alcántara and S. C. E. Tsang, *ACS Energy Lett.*, 2022, **7**, 1021–1033.
8 H. Liu, *Chin. J. Catal.*, 2014, **35**, 1619–1640.
9 A. Braun, D. K. Bora, L. Lauterbach, E. Lettau, H. Wang, S. P. Cramer, F. Yang and J. Guo, *Catal. Today*, 2022, **387**, 186–196.
10 J. Sehested, C. J. H. Jacobsen, E. Törnqvist, S. Rokni and P. Stoltze, *J. Catal.*, 1999, **188**, 83–89.
11 J. Guo and P. Chen, *Chin. Sci. Bull.*, 2019, **64**, 1114–1128.
12 Z. Zhang, Y. Jiang, J. Li, M. Miyazaki, M. Kitano and H. Hosono, *J. Am. Chem. Soc.*, 2023, **145**, 24482–24485.
13 A. Ozaki, *Acc. Chem. Res.*, 1981, **14**, 16–21.
14 M. Kitano, Y. Inoue, Y. Yamazaki, F. Hayashi, S. Kanbara, S. Matsuishi, T. Yokoyama, S.-W. Kim, M. Hara and H. Hosono, *Nat. Chem.*, 2012, **4**, 934–940.
15 Y. Gong, J. Wu, M. Kitano, J. Wang, T.-N. Ye, J. Li, Y. Kobayashi, K. Kishida, H. Abe, Y. Niwa, H. Yang, T. Tada and H. Hosono, *Nat. Catal.*, 2018, **1**, 178–185.
16 J. Kammert, J. Moon, Y. Cheng, L. Daemen, S. Irle, V. Fung, J. Liu, K. Page, X. Ma, V. Phaneuf, J. Tong, A. J. Ramirez-Cuesta and Z. Wu, *J. Am. Chem. Soc.*, 2020, **142**, 7655–7667.
17 K. Zhang, A. Cao, L. H. Wandall, J. Vernieres, J. Kibsgaard, J. K. Nørskov and I. Chorkendorff, *Science*, 2024, **383**, 1357–1363.
18 Y. Wang, M. Craven, X. Yu, J. Ding, P. Bryant, J. Huang and X. Tu, *ACS Catal.*, 2019, **9**, 10780–10793.
19 P. M. Barboun, H. O. Otor, H. Ma, A. Goswami, W. F. Schneider and J. C. Hicks, *ACS Sustainable Chem. Eng.*, 2022, **10**, 15741–15748.
20 T.-N. Ye, S.-W. Park, Y. Lu, J. Li, M. Sasase, M. Kitano and H. Hosono, *J. Am. Chem. Soc.*, 2020, **142**, 14374–14383.
21 T.-N. Ye, S.-W. Park, Y. Lu, J. Li, M. Sasase, M. Kitano, T. Tada and H. Hosono, *Nature*, 2020, **583**, 391–395.
22 T.-N. Ye, S.-W. Park, Y. Lu, J. Li, J. Wu, M. Sasase, M. Kitano and H. Hosono, *J. Am. Chem. Soc.*, 2021, **143**, 12857–12866.
23 Y. Lu, T. Ye, J. Li, Z. Li, H. Guan, M. Sasase, Y. Niwa, H. Abe, Q. Li, F. Pan, M. Kitano and H. Hosono, *Angew. Chem., Int. Ed.*, 2022, **61**, e202211759.
24 Y. Tang, S. Zhao, B. Long, J.-C. Liu and J. Li, *J. Phys. Chem. C*, 2016, **120**, 17514–17526.
25 Y. Abghoui, A. L. Garden, J. G. Howalt, T. Vegge and E. Skúlason, *ACS Catal.*, 2016, **6**, 635–646.
26 Y. Abghoui and E. Skúlason, *J. Phys. Chem. C*, 2017, **121**, 6141–6151.
27 Y. Abghoui and E. Skúlason, *Catal. Today*, 2017, **286**, 78–84.
28 C. D. Zeinalipour-Yazdi, J. S. J. Hargreaves and C. R. A. Catlow, *J. Phys. Chem. C*, 2018, **122**, 6078–6082.
29 K. Feng, J. Tian, J. Zhang, Z. Li, Y. Chen, K. H. Luo, B. Yang and B. Yan, *ACS Catal.*, 2022, **12**, 4696–4706.
30 R. D. Cortright and J. A. Dumesic, in *Advances in Catalysis*, Elsevier, 2001, vol. 46, pp. 161–264.
31 D. G. Blackmond, *Angew. Chem., Int. Ed.*, 2005, **44**, 4302–4320.

32 R. J. Berger, F. Kapteijn, J. A. Moulijn, G. B. Marin, J. De Wilde, M. Olea, D. Chen, A. Holmen, L. Lietti, E. Tronconi and Y. Schuurman, *Appl. Catal., A*, 2008, **342**, 3–28.
33 N. C. Nelson, M.-T. Nguyen, V.-A. Glezakou, R. Rousseau and J. Szanyi, *Nat. Catal.*, 2019, **2**, 916–924.
34 F. Polo-Garzon, V. Fung, L. Nguyen, Y. Tang, F. Tao, Y. Cheng, L. L. Daemen, A. J. Ramirez-Cuesta, G. S. Foo, M. Zhu, I. E. Wachs, D. Jiang and Z. Wu, *J. Am. Chem. Soc.*, 2019, **141**, 7990–7999.
35 C. J. H. Jacobsen, S. Dahl, B. S. Clausen, S. Bahn, A. Logadottir and J. K. Nørskov, *J. Am. Chem. Soc.*, 2001, **123**, 8404–8405.
36 R. Kojima and K. Aika, *Appl. Catal., A*, 2001, **209**, 317–325.
37 B. McClaine, *J. Catal.*, 2002, **210**, 387–396.
38 S. Siporin, *J. Catal.*, 2004, **222**, 315–322.
39 Y. Kobayashi, M. Kitano, S. Kawamura, T. Yokoyama and H. Hosono, *Catal. Sci. Technol.*, 2017, **7**, 47–50.
40 A. J. Medford, J. Wellendorff, A. Vojvodic, F. Studt, F. Abild-Pedersen, K. W. Jacobsen, T. Bligaard and J. K. Nørskov, *Science*, 2014, **345**, 197–200.
41 W. Chen, J. Cao, J. Yang, Y. Cao, H. Zhang, Z. Jiang, J. Zhang, G. Qian, X. Zhou, D. Chen, W. Yuan and X. Duan, *Nat. Commun.*, 2021, **12**, 6888.
42 X. Wang, D. Li, Z. Gao, Y. Guo, H. Zhang and D. Ma, *J. Am. Chem. Soc.*, 2023, **145**, 905–918.
43 T. Pu, A. Setiawan, A. C. Foucher, M. Guo, J.-M. Jehng, M. Zhu, M. E. Ford, E. A. Stach, S. Rangarajan and I. E. Wachs, *ACS Catal.*, 2024, **14**, 406–417.
44 C. D. Zeinalipour-Yazdi, J. S. J. Hargreaves and C. R. A. Catlow, *J. Phys. Chem. C*, 2015, **119**, 28368–28376.
45 C. D. Zeinalipour-Yazdi, J. S. J. Hargreaves and C. R. A. Catlow, *J. Phys. Chem. C*, 2016, **120**, 21390–21398.
46 S. Qian, K. Feng, Z. Li, Y. Chen, X. Sun, Y. Wang, B. Yan and Y. Cheng, *ACS Catal.*, 2023, **13**, 13931–13940.
47 J.-C. Liu, X.-L. Ma, Y. Li, Y.-G. Wang, H. Xiao and J. Li, *Nat. Commun.*, 2018, **9**, 1610.
48 B. Rösch, T. X. Gentner, J. Langer, C. Färber, J. Eyselein, L. Zhao, C. Ding, G. Frenking and S. Harder, *Science*, 2021, **371**, 1125–1128.
49 A. Logadottir, T. H. Rod, J. K. Nørskov, B. Hammer, S. Dahl and C. J. H. Jacobsen, *J. Catal.*, 2001, **197**, 229–231.
50 R. Michalsky, A. M. Avram, B. A. Peterson, P. H. Pfromm and A. A. Peterson, *Chem. Sci.*, 2015, **6**, 3965–3974.
51 J. K. Nørskov, T. Bligaard, J. Rossmeisl and C. H. Christensen, *Nat. Chem.*, 2009, **1**, 37–46.
52 J. Pérez-Ramírez and N. López, *Nat. Catal.*, 2019, **2**, 971–976.
53 A. Ozaki, H. S. Taylor and M. Boudart, *Proc. R. Soc. London, Ser. A*, 1960, **258**, 47–62.

